

管道对接间断焊与连续焊的有限元分析

张国栋, 周昌玉

(南京工业大学 机械与动力工程学院, 南京 210009)



张国栋

摘 要: 应用大型有限元分析软件 ABAQUS, 对工业管道间断焊与连续焊的温度场和残余应力场进行数值模拟。考虑材料的物理性能随温度的变化以及外界环境对焊接构件温度场的影响, 采用热振幅曲线加载方法模拟焊接热源的移动, 运用单元生死技术实现管道多道焊的模拟。将两种焊接工艺得到的温度场和残余应力场进行比较。结果表明, 间断焊可以降低焊接时的温度, 而采用连续焊可以获得较小的轴向残余应力, 间断焊和连续焊的环向应力对管道的影响不大。另外对起焊点处的温度场和残余应力场也做了详细的分析, 起焊点内壁处的轴向残余应力较大。

关键词: 间断焊; 连续焊; 温度场; 残余应力场; 数值模拟

中图分类号: TG404 文献标识码: A 文章编号: 0253-360X(2006)12-085-05

0 序 言

管道是物料输送的一种特殊设备^[1], 在石化生产装备中管道的安装工作量约占整个工作量的 1/2, 因管道失效造成重大损失的例子也是屡见不鲜的。焊接成形后, 残余应力是影响这些构件安全运行的重要因素之一, 采用不同的焊接工艺得到的残余应力会有所不同。目前国内外管道焊接模拟工作主要集中在管道对接^[2,3]和 T 形接管^[4]的焊接, 管道带压开孔间断焊的数值模拟工作在国内已开展^[5], 但对管道对接焊间断焊与连续焊的数值模拟等研究工作有待深入开展。

连续焊就是在焊接过程中以不间断加热的方式连续完成; 间断焊, 即采用焊接—冷却—焊接的方法进行焊接。文中的计算模型为接管, 分别采用间断焊和连续焊两种焊接工艺。运用大型有限元软件 ABAQUS^[6], 建立三维实体模型, 运用单元生死技术对管道对接多道焊实现焊接温度场的模拟, 通过热—力耦合功能实现残余应力场的模拟, 获取残余应力的分布规律。

1 物理模型

研究的对象是直径为 $\Phi 70$ mm, 壁厚为 4 mm 的管道对接焊接头, 管道材料为 316L。焊缝开坡口, 采用焊条电弧焊, 分两道焊接成形, 焊接结束后冷却到

常温。焊接接头见图 1, 接管焊接参数见表 1。间断焊每焊接 110 mm 冷却 200 s。连续焊与间断焊第一道焊结束后要进行清渣等工作, 需花 200 s 时间。

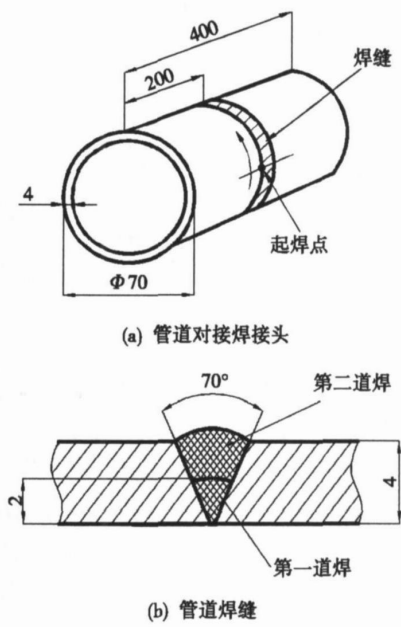


图 1 管道对接焊接头和管道焊缝 (mm)
Fig. 1 Pipe butt joint and weld

表 1 焊接工艺参数

Table 1 Welding parameters

焊道	焊条直径 <i>d</i> /mm	焊接电流 <i>I</i> /A	电弧电压 <i>U</i> /V	焊接速度 <i>v</i> /(m·h ⁻¹)
1	2.5	90~110	22~25	7~8
2	3.2	140~160	23~26	8~9

2 有限元分析步骤

2.1 计算模型

由于是等径管道对接焊, 利用对称条件, 以焊接中心面为对称面, 建立模型。该模型采用 8 节点三维实体单元, 利用 ABAQUS 软件的网格自适应处理的特点^[6], 在靠近焊缝处热影响区部位对网格进行细分, 在远离焊缝处加大网格。有限元网格划分见图 2 所示。温度场分析时, 单元类型为热单元 (DC3D8), 残余应力场分析时, 单元类型为力分析单元 (C3D8)。

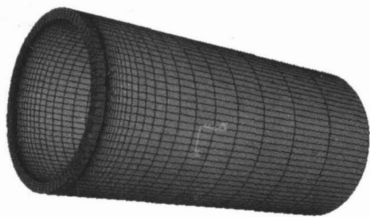


图 2 有限元模型网格划分
Fig. 2 Mesh of finite element model

2.2 材料模型

316L 不锈钢的热力学和热化学性质参照文献 [7]。1 420 °C 为 316L 不锈钢的固相线温度, 1 460 °C 为 316L 不锈钢的液相线温度。在焊接加热的过程中, 要考虑相变的影响^[8], 由于材料的熔化需要吸收大量的热, 而当焊后凝固时则需要放热, 因此需要考虑焊接熔池相变潜热对焊接温度场的影响。由文献 [7] 可知, 取 316L 不锈钢的潜热为 300 kJ/kg。

2.3 焊接热源

采用高斯热源模型, 高斯热源分布比点状热源和线状热源更符合实际情况的热源分布函数, 对焊接的热输入模拟更加精确^[9]。高斯模型的能流密度为

$$q^* = q_{\max} \exp(-\alpha^2), \tag{1}$$

式中: q^* 为高斯热源半径 r 处的热流密度; q_{\max} 为最大体热流密度; c 为热源集中系数, 与焊接方法相关的常数; r 为距热源中心的距离。

以焊接体热源形式加载至焊缝单元, 通过热流的振幅曲线将热量逐个加上去。运用单元生死技术逐层将焊接热输入加上去。最大体热流密度计算公式如下, 即

$$q_{\max} = \frac{\eta U}{\pi abh}, \tag{2}$$

式中: η 为电弧热效率, 其值在 0.7 ~ 0.9, 文中取 0.85; I 为焊接电流; U 为电弧电压; a, b 表示高斯热源中椭圆的长短轴; h 为焊缝高度。将式 (2) 代入 (1) 式中即可得到焊接热源的体热流密度。

2.4 边界条件

在热场分析中, 焊件的初始温度取室温, 文中取 20 °C, 管道的内外表面均考虑为对流和辐射的边界条件, 对流系数取 10 W/(m²K), 辐射发射率为 0.85^[10]。

在应力场分析中, 管道焊缝中心面为对称面, 加对称约束, 另外为了确保焊件不发生刚性移动, 在有限元模型中, 远离焊缝处任取两节点固定。

3 数值模拟结果与分析

3.1 焊接温度场

焊接温度场是进行残余应力分析的基础, 取靠近焊缝上的一点 (距起焊点 90°) 和起焊点, 做出间断焊和连续焊的热循环曲线, 如图 3, 图 4 所示。

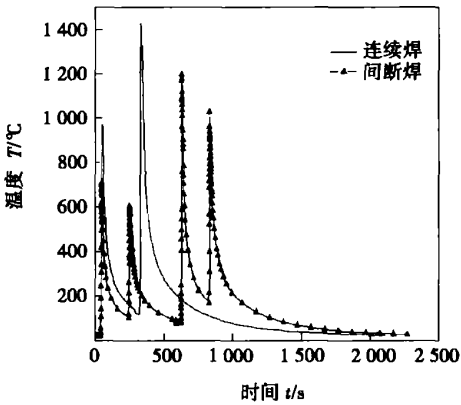


图 3 间断焊与连续焊的热循环曲线
Fig. 3 Discontinuous and continuous welding therm-cycle curve

3.1.1 管道焊接到距起焊点 90° 的温度场

由图 3 可以看出同一点间断焊的峰值温度低于连续焊的峰值温度。连续焊接为连续加热, 该点的温度随热源的移动而不断升高而达到峰值, 同时又随着热源的离开而逐渐降低, 由于采取两道焊焊接管道, 故连续焊的热循环曲线出现两个峰值, 并且离的很近; 间断焊接时, 它的热积累没有连续焊的程度大, 因此峰值温度也就自然低于连续焊的峰值温度, 间断焊热循环曲线的特点就是多次出现峰值, 且峰值温度明显低于连续焊的峰值温度。另外, 连续焊出现了 2 次峰值温度, 而间断焊出现了 4 次峰值温

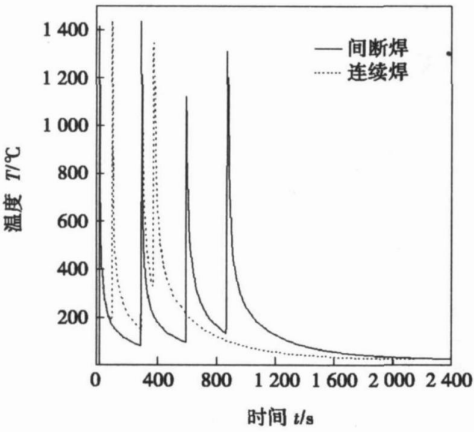


图 4 间断焊与连续焊起焊点热循环曲线
Fig. 4 Discontinuous and continuous welding therm-cycle curve at initial welding point

度。

3.1.2 起焊点温度场

由于管道焊接起焊点温度场的特殊性, 故取起焊点做其热循环曲线分析, 由图 4 可以看出, 由于起焊点热输入相同, 间断焊和连续焊起点的热循环曲线的峰值温度基本相同, 只是焊接总时间不同。另外由于管道焊接的起焊点又是焊接的终点, 故两道焊焊接起点处出现了 4 次峰值, 这与管道其它位置的热循环曲线是不同的。

3.2 焊接接头残余应力场

3.2.1 管道焊接过程中的残余应力场

图 5 为距起焊点 120°和 80°时间间断焊与连续焊外壁与内壁的轴向残余应力。间断焊外壁轴向表现为拉应力, 到距焊缝 20 mm 处为最大, 230 MPa, 而后拉应力逐渐减小, 到130 mm处减小为零; 连续焊外

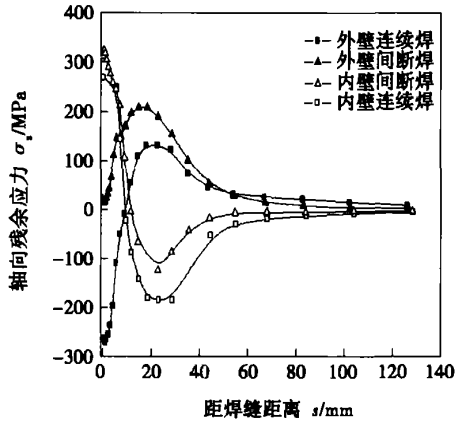


图 5 间断焊与连续焊内外壁轴向残余应力
Fig. 5 Outer and Inner wall axial residual stress of discontinuous and continuous welding

壁轴向距焊缝近端表现为压应力, 最大压应力为 273 MPa, 在距焊缝 12 mm 以后为拉应力随着距焊缝距离的增大而逐渐减小; 间断焊与连续焊内壁距焊缝最近处的残余应力均为拉应力, 间断焊为 327 MPa, 连续焊为 270 MPa, 随着距焊缝距离的增大拉应力逐渐转化为压应力, 在距焊缝 23 mm 处间断焊的压应力为 125 MPa, 连续焊的压应力为 200 MPa。

图 6 为距起焊点 200°和 280°时外壁与内壁环向残余应力。可以看出间断焊和连续焊的外壁环向残余应力曲线基本吻合。用这两种焊接工艺得到的外壁环向应力均表现为拉应力, 在距焊缝 5 mm 处拉应力最大, 为 112 MPa; 间断焊内壁环向残余应力明显大于连续焊的。在距焊缝 4 mm 间断焊环向拉应力最大, 达到 115 MPa, 而后随着离焊缝的距离增大而逐渐减小为零; 连续焊的环向残余应力在距焊缝 25 mm 以内, 拉压应力在 40 MPa 附近波动。

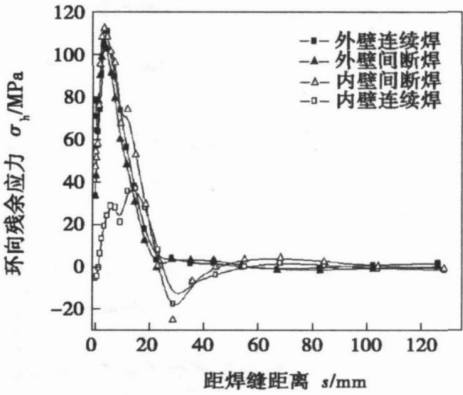


图 6 间断焊与连续焊内外壁环向残余应力
Fig. 6 Outer and Inner wall annular residual stress of discontinuous and continuous welding

3.2.2 起焊点处的残余应力场

由于起焊点温度场的特殊性, 应力场也会有相应的变化。图 7, 图 8 分别为起焊点外壁和内壁的轴向和环向残余应力分布。由此看出, 连续焊起焊点内壁和外壁距离焊缝最近处的轴向残余拉压应力均大于间断焊起焊点该处的轴向应力, 连续焊外壁轴向最大残余拉压应力为 170 MPa; 内壁最大拉应力为 330 MPa, 压应力较小为 70 MPa。间断焊外壁轴向应力曲线几乎与连续焊相同; 内壁最大拉应力为 300 MPa。间断焊和连续焊起焊点轴向残余应力的分布规律一致。内外壁环向应力分布规律和大小基本一致, 起焊点外壁环向应力均表现为压应力, 最大值为 130 MPa, 内壁表现为拉应力, 最大值为 97 MPa。

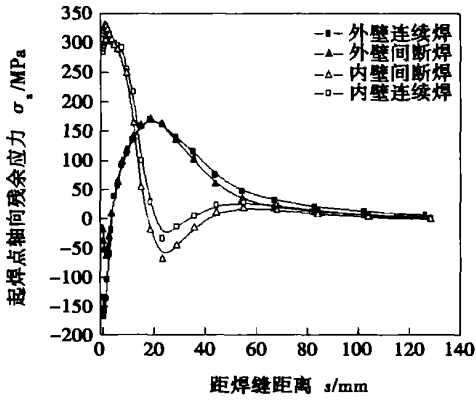


图 7 间断焊与连续焊起焊点内外壁轴向残余应力
Fig. 7 Outer and Inner wall axial residual stress of discontinuous and continuous welding at initial welding point

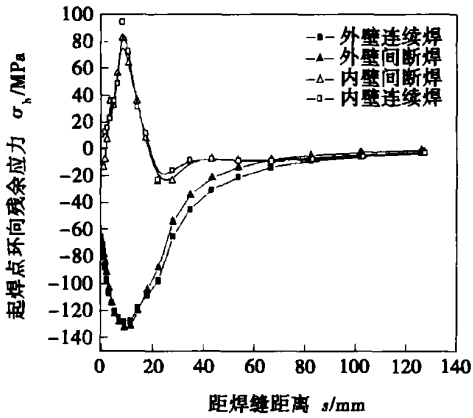


图 8 间断焊与连续焊起焊点内外壁环向残余应力
Fig. 8 Outer and Inner wall annular residual stress of discontinuous and continuous welding at initial welding point

3.2.3 管道焊接过程中的应力场与起焊点处应力场的比较

将图 5、图 6 与图 7、图 8 对比,起焊点的外壁轴向应力明显小于焊接过程中的残余应力,而起焊点的内壁残余应力与焊接过程中一点的应力分布规律和大小基本一致,内壁处的起焊点的应力是焊后热处理应该特别注意的一点。起焊点外壁环向应力均为压应力,而焊接过程中的外壁环向应力均为拉应力,且这两者的环向拉压应力都在 140 MPa 以内,应力值不大。间断焊起焊点内壁环向应力比焊接过程中的内壁环向应力小 30 MPa,而连续焊起焊点内壁环向应力比焊接过程中的内壁环向应力大 55 MPa。但二者环向应力最大值为 115 MPa,因此,环向应力对整体焊接结构的影响不大。

4 结果验证

将连续焊分析结果与文献[3]的管道多道焊的试验点结果相比较,如图 9 所示。

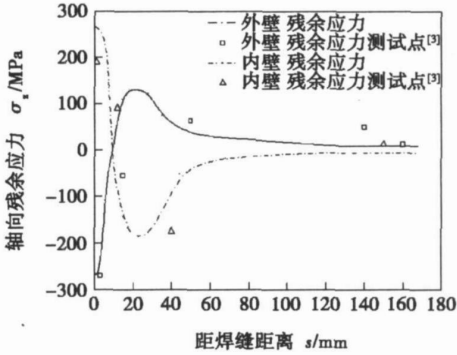


图 9 轴向应力的试验点与模拟结果比较
Fig. 9 Comparison between experimental and numerical results on axial residual stress

引用文献[3]的试验点,文献中的焊接模型是 $\Phi 812.8 \text{ mm} \times 15.9 \text{ mm}$ 管道的焊接,和文中的模型相比均属于薄壁管道的焊接,试验点的轴向应力分布和文中一致。另由文献[11]可知,当管道壁较薄,直径较小时,环向应力可以小到忽略不计的程度,在一定条件下甚至变为负值(压应力)。图 6 的环向应力分布及大小与此结论一致。

5 结 论

- (1) 采用间断焊可有效的降低焊接时焊缝区的温度,降低层间温度。
 - (2) 采用间断焊焊接管道轴向最大应力均表现为拉应力,而且在内壁热影响区的轴向拉应力达到了最大 327 MPa 时,超过的管材 316L 不锈钢的屈服极限。而连续焊得到的最大残余压应力在外壁处,为 273 MPa。
 - (3) 起焊点处连续焊的轴向残余应力大于间断焊,且内壁最大应力达到 330 MPa。而起焊点处环向应力则较小,因此在焊接过程中起焊点轴向应力的状况值得关注。
 - (4) 间断焊和连续焊对管道环向应力的影响都不大,而且其残余应力的分布也基本相同。因此,在为了降低管道局部焊接温度的情况下建议采用间断
- [下转第 92 页]

- (2) 焊接接头 Ti、Ni 元素的分布没有发生明显的偏移,焊缝组织粗大,有少量新相析出。
- (3) 焊后未经处理的焊缝相变点变化杂乱,经 500 ℃热处理后焊缝相变点变得清晰;且焊接接头形状记忆性能达到了母材的 93.8%。
- (4) 常温下,焊接接头抗拉强度是母材抗拉强度的 62.2%。
- (5) 采用等离子焊接记忆合金与钨极氩弧焊方法比较,能量更加集中,焊缝与热影响区更加窄;与激光焊、电子束焊接方法比较,设备简单,可操作性强,应用前景宽广。

参考文献:

[1] 韩立军,赵熹华. TiNiNb 形状记忆合金丝精密脉冲电阻对焊工艺分析[J]. 材料科学与工艺, 1999, 7(3): 76—79.

[2] Li M G, Sun D Q, Qiu X M, *et al.* Effects of laser brazing parameters on microstructure and properties of TiNi shape memory alloy and stain-

less steel joint [J]. Materials Science and Engineering A, 2006, 424 (1): 17—22.

[3] 广濑明夫. Ti-Ni 系形状记忆合金的熔接[J]. 金属, 1990, 59 (8): 61—68.

[4] Ikai A, Kimura K, Tobushi H. TIG welding and shape memory effect of TiNi shape memory alloy [J]. Journal of Intelligent Material Systems and Structures, 1996, 11(7): 646—655.

[5] 吴 冶, 孟祥龙. Ni47Ti44Nb9 合金丝氩弧焊接头的显微组织和力学行为[J]. 材料科学与工艺, 2005, 13(3): 312—315.

[6] 郭立伟. 形状记忆合金 CuAlZn 的扩散焊接头组织性能 [J]. 中国有色金属学报, 2003, 13(2): 404—408.

[7] 薛松柏. TiNi 形状记忆合金电阻钎焊技术[J]. 焊接学报, 2004, 25(1): 1—5.

[8] 赵熹华, 韩立军, 赵 蕾. 随机后热处理对 TiNi 记忆合金精密脉冲电阻对焊接头性能的影响[J]. 焊接学报, 2001, 22(1): 1—5.

作者简介:徐越兰, 女, 1952 年 11 月出生, 教授。主要从事新材料的焊接、焊接材料智能化设计的研究, 发表论文 30 余篇。
Email: xuyuelan33@sina.com

[上接第 88 页]

焊,但要采取良好的局部热处理方法降低间断焊内壁以及起焊点处的轴向残余应力。

参考文献:

[1] 顾纪清, 阳代军. 管道焊接技术[M]. 北京: 化学工业出版社, 2005.

[2] 金晓军, 霍立兴, 张玉凤, 等. 双相不锈钢管道全位置焊接残余应力三维有限元数值模拟[J]. 焊接学报, 2004, 25(2): 52—56.

[3] Dong P, Brust F W. Welding residual stress and effects on fracture in pressure vessel and piping components: a millennium review and beyond [J]. Journal of Pressure Vessel Technology, 2000, 12(8): 329—338.

[4] 蔡洪能, 张国栋, 王雅生. 厚壁压力容器接管的三维有限元分析 [J]. 焊管, 1999, 22(5): 11—14.

[5] 薛小龙, 桑芝富, 姜卫忠. 带压开孔结构多道间断焊的数值模 [J]. 焊接学报, 2005, 26(4): 25—28.

[6] H K S Inc. Abaqus user's manual (Version 6.2) [M]. USA: Providence, RI, 2000.

[7] Dong P. Residual stress analyses of a multi-pass girth weld: 3-D special shell versus axisymmetric models[J]. Journal of Pressure Vessel Technology, 2001, 123(5): 207—213.

[8] 蔡洪能, 唐慕尧. TIG 焊接温度场的有限元分析[J]. 机械工程学, 1996, 32(2): 34—39.

[9] 董志波, 魏艳红, 刘仁培. 不锈钢焊接温度场的三维数值模拟 [J]. 焊接学报, 2004, 25(2): 9—14.

[10] 倪红芳, 凌 祥, 涂善东. 多道焊残余应力场三维有限元模拟 [J]. 机械强度, 2004, 26(2): 218—222.

[11] 宋天民. 焊接残余应力的产生与消除[M]. 北京: 中国石化出版社, 2005.

作者简介:张国栋, 男, 1982 年出生, 博士研究生。主要从事过程装备的可靠性、寿命预测的研究, 已发表论文 2 篇。
Email: zhangdln@163.com

and DP600. Artificial neural networks(ANN)are used to describe the mapping relationship between welding parameters and welding quality. After analyzing the limitation of standard BP networks, the original model was optimized based on lots of experiments. Then a lot of experimental data about welding parameters and corresponding spot welding quality were supplied to the ANN for training. The results indicate that the improved BP network model can accurately predict the influence of welding currents on welding nugget diameters, depth of indentation and the tension-shear strength of welding spots. That is to say, the model can effectively predict the spot welding performance of the galvanized steel sheets. The forecasting precision is high enough to meet the practical need of engineering and has some application value.

Key words: body galvanized steel sheet; spot welding; artificial neural networks; prediction; optimization

Effects of uneven surface on ultrasonic testing results of defects

close to surface GUO Li-wei, Gang Tie, Hu xin(State Key Laboratory of Advanced Welding Production Technology, Harbin Institute of Technology, Harbin 150001, China). p81—84

Abstract: Laser welding is an important method to join titanium alloy. The rigorous nondestructive test is necessary because pores are easily formed in the laser welding. The bad effects of uneven weld surface on the automatic ultrasonic inspection were summarized. The simulated practical sample was inspected through immersed ultrasonic testing technique at different point with different frequency probe. The defects images of weld were constructed using reasonable testing parameters and probe. The defect, which was located in 1.0-2.5 mm below the surface and whose diameter was bigger than 0.3 mm, can be detected, when the testing process was used to detect the T-shape Ti alloy laser welded joint. The experimental results show that a right frequency of probe can reduce the bad influence of uneven surface, which improves the reliability of ultrasonic test effectively.

Key words: immersed ultrasonic test; laserwelding; Ti alloy T joint; C-scan

Finite element analysis of pipe discontinuous and continuous butt welding

ZHANG Guo-dong, ZHOU Chang-yu(College of Mechanical and Power Engineering, Nanjing University of Technology, Nanjing 210009, China). p85—88, 92

Abstract: Temperature and residual stress fields of industrial pipe discontinuous and continuous butt welding was simulated by ABAQUS. The physical properties of the material depend on the temperature, and the effects of environmental conditions on welding temperature field which were both considered in simulation. The heat amplitude curves loading method was applied to simulate the moving heat source. The multi-pass welding was simulated by the technique of element birth and death. A comparison of temperature and residual stress fields between discontinuous and continuous welding was carried out. Results indicated that the temperature was much lower while discontinuous welding, but lower axial residual stress can be gained by continuous welding. The annular stress of discontinuous and continuous welding did not have much affection for the pipeline.

In addition, the temperature and residual stress field of starting welding point was analyzed. The inner wall residual stress was much higher in starting welding point.

Key words: discontinuous weld; continuous weld; temperature field; stress field; numerical simulation

Plasma beam welding of shape memory alloy XU Yue-lan¹, CHENG Zhi-fu¹, FAN Xiao-long¹, CHU Cheng-lin², WANG Shidong²(1. Department of Material Science and Technology, Nanjing University of Science and Technology, Nanjing 210094, China; 2. Material School, Southeast University, Nanjing 210006, China). p89—92

Abstract: With high-energy plasma beam method, the weldability of the TiNi shape memory alloy sheet was studied. The high-energy plasma beam equipment system was partly designed and founded. The relationship among parameters and its proper adjusting range are acquired. Thus the range of the parameters used in the engineering application was obtained. Some characteristics such as phase, microstructure, shape memory properties and tensile strength of the welded joint were discussed. Results show that the crystal grain in welded joint is large, and new phases such as Ni₃Ti and Ti₂Ni separate out. Furthermore, the welding heat-affected zone is narrow, and the welded joint shape restoration rate is 93.8% of the parent metal and the parent metal tensile strength is 1 205 MPa. After being kept at 500 °C for 1 hour, the tensile strength of welded joint reaches 750 MPa which is 62.2% of the parent metal and the fracture appears in the center of weld.

Key words: shape memory alloy; plasma beam; heat treatment

Analysis on welding cold crack sensibility of 10Ni8CrMoV steel

DU Yi, ZHANG Tian-hong, ZHANG Jun-xu(Luoyang Ship Material Research Institute, Luoyang 471039, Henan, China). p93—96

Abstract: By using implant test, cold cracking sensibility of 10Ni8CrMoV high strength steel was analysed. At four welding conditions of non-preheating, preheating at 100 °C, preheating at 150 °C and preheating at 150 °C then postheating 200 °C×2 h, the critical rupture stresses of implant test and the welding thermal cycling parameters were measured, and the fracture appearance were observed by scanning electron microscope. By all these, the welding cold crack sensibility of 10Ni8CrMoV steel was analysed comprehensively. The results showed that with the preheat temperature being increased, the critical rupture stresses of implant test are higher, and the areas of dimple are relatively increasing in fracture surfaces, and the rupture tendency is displayed from intergranular crack to transgranular crack to ductile rupture. 10Ni8CrMoV steel possesses a high cold cracking sensibility. Preheat and postheat treatment technologies can obviously improve the weldability of 10Ni8CrMoV steel.

Key words: 10Ni8CrMoV steel; implant test; cold crack sensibility; critical rupture stress

Fatigue properties improvement of welded structures by plasma spraying process WANG Bing-ying, HUO Li-xing, WANG